Taylor & Francis
Taylor & Francis Group

Mechanics of Advanced Materials and Structures

ISSN: 1537-6494 (Print) 1537-6532 (Online) Journal homepage: http://www.tandfonline.com/loi/umcm20

XFEM fracture analysis of cracked pipeline with and without FRP composite repairs

Z. Valadi, H. Bayesteh & S. Mohammadi

To cite this article: Z. Valadi, H. Bayesteh & S. Mohammadi (2018): XFEM fracture analysis of cracked pipeline with and without FRP composite repairs, Mechanics of Advanced Materials and Structures, DOI: 10.1080/15376494.2018.1529844

To link to this article: https://doi.org/10.1080/15376494.2018.1529844

Published online: 31 Dec 2018.

MECHANICS OF ADVANCED MATERIALS AND STRUCTURES
https://doi.org/10.1080/15376494.2018.1529844

Taylor & Francis
Taylor & Francis Group

ORIGINAL ARTICLE

XFEM fracture analysis of cracked pipeline with and without FRP composite repairs

Z. Valadi, H. Bayesteh, and S. Mohammadi

High Performance Computing Lab, School of Civil Engineering, Faculty of Engineering, University of Tehran, Tehran, Iran

ABSTRACT

The effect of fiber reinforced polymer composite (FRPC) repair on crack propagation in thin-walled steel pipes is examined. The extended finite element method is used in this study to simulate a pressurized cylindrical pipe with longitudinal crack in two conditions: the original cracked pipe and the pipe repaired with a composite patch. Carbon/epoxy or E-glass/epoxy FRP in two different fiber orientations are assumed for cracked pipe repair. Performance of four types of FRP repair systems are investigated by CTOA, COD and COA fracture criteria for both the pipe integrity assessment and the potential age of leak before break criterion.

ARTICLE HISTORY
Received 18 July 2018
Accepted 25 September 2018

KEYWORDS
XFEM; fracture; FRP repair; pressurized pipe; crack propagation

Nomenclature

$\mathbf{b}_k^l$	Vector of additional degrees of freedom for modeling the crack tip
$\mathbf{d}$	Vector of nodal displacements
$\mathbf{D}$	Material modulus matrix
F_l	In plane enrichment function
$\mathbf{f}$	Vector of nodal forces
G_i	Unit vector at node i
G_l	Rotational tip enrichment functions
h_i	Shell thickness at node i
$H(\phi)$	Heaviside function
$\mathbf{k}$	Stiffness matrix
M_i	One dimensional shape function
$\mathbf{n}$	Normal vector
N_i	FE shape functions
R_l	Out of plane enrichment functions
r, s, t	Local Cartesian coordinate system
u^h	Displacement field
u^{FE}	Classical finite element displacement field
u^{enr}	The enriched part of the displacement field
$\hat{\mathrm{u}}_i$	Nodal displacements
$\mathbf{u}$	Vector of displacement field
$\mathbf{x}^{top}$	Geometry at the top of shell
$\mathbf{x}^{bot}$	Geometry at the bottom of shell
X	Geometry of shell elements
$\xi(\mathbf{x})$	Signed distance function
$\hat{\alpha}_i$	Rotation with respect to $\mathbf{e}_{2i}$
$\hat{\beta}_i$	Rotation with respect to $\mathbf{e}_{1i}$
θ_i^{α}	Rotational DOFs with respect to $\mathbf{e}_{2i}$
γ_i^{β}	Rotational DOFs with respect to $\mathbf{e}_{1i}$

1. Introduction

Steel tubular sections, the most common elements in oil and gas industries, are among the efficient means of hydrocarbon fluid transportation from one place to another. Onshore and offshore pipelines can be subjected to different load combinations and suffer from different damage and failure mechanisms in their lifetime. Damage in pipelines can be originated from internal or external damages such as corrosion, erosion, dents and cracks. Existence of cracks may cause load capacity reduction, fluid leakage before breakage and even structural collapse. Appropriate repairs are, therefore, necessary to maintain the structural integrity and operation of pipeline systems toward the end of their design service life. Common repair methods such as clamps or sleeves are welded or bolted around the damaged zone. Transporting heavy clamp systems to the operation fields, especially in offshore structures, welding to an operating pipeline, and installation expenses are some of major challenges of these methods.

On the other hand, industries have widely accepted the FRP composite repair technique for strengthening and repair of various types of structures as an alternative efficient approach to the conventional methods [1]. Composite materials are light and do not require welding or bolting, so their installation is relatively simple. In many researches, FRP composite has been externally applied on various steel members to improve the structural performance [2, 3]. Majority of these studies have focused on reinforcing tubular and hollow sections. High strength FRPs can easily be implemented, and increasingly adopted for retrofitting and strengthening of steel tubular joints, inshore and onshore systems and offshore pipelines [4–6].

More recently, different investigations on steel pipeline repairs with FRP have been performed. Among them, an experimental study of behavior of FRP repaired pipelines under different loading conditions was compared with the finite element results by Shouman and Taheri [7]. Costa

CONTACT Sohell Mohammadi smoham@ut.ac.ir High Performance Computing Lab, School of Civil Engineering, Faculty of Engineering, University of Tehran, Tehran, Iran.
Color versions of one or more of the figures in the article can be found online at www.tandfonline.com/umcm.

et al. [8] suggested a simple methodology to indicate the failure pressure and define the necessary FRP repair thickness of a thin-walled corroded pipe. Moreover, Shdlou and Taheri [9] performed an FEM analysis of repaired pipe under combined loading to investigate the effects of geometry of composite layer and imperfect interface between the pipe and repair wrap on the loading capacity.

FRP repair systems have also been used as a repair method for offshore pipelines, bridges and platform jackets. Alexander and Ochoa [5] designed a carbon/epoxy based composite repair system to extend this method to offshore steel risers. Moreover, Alexander [10] used a full-scale test program to assess the performance of composite repair method in offshore pipelines and risers. Experimental and numerical studies on the behavior of FRP rehabilitation of steel tubular connections were carried out by Lesani et al. [11].

Parametric studies are necessary to investigate the FRP repaired pipe behavior and to choose the appropriate type of FRP system as a repair solution for the damaged pipeline. Chan et al. [12, 13] studied the stress-strain response of a pipe riser in three conditions: uncorroded, corroded, and repaired corroded pipe with FRP through FE and experimental testing. They determined the most effective FRP repair system and the minimum required thickness of FRP in comparison with ASME PCC-2 [14].

Furthermore, cracks may develop and propagate in pressure vessels and pipelines which carry oil and gas. Accordingly, choosing the best repair system is necessary to maintain the structural integrity of pressure pipelines. Recent researches indicate that using the FRP composite repair method is an efficient way for repairing these cracked structures by potentially increasing the service-life and diminishing the stress intensity factor. Hosseini-Toudeshky and Fadaei [15] used FEM to investigate composite wrap thickness and length on a repaired pipe with an internal longitudinal crack, and the effect of circumferential crack size on the stress intensity factor in a composite repaired pipe was carried out by a three dimensional finite element method [16, 17]. Meriem-Benziane [18] used FEM analysis to study the performance of composite repair wrap on the stress intensity factor of an API X65 pipeline with a longitudinal crack.

While most of the previous studies on the cracked pipes repaired with FRP utilized FEM with the 3D brick elements to model pipes, shell elements were also used for fracture analysis of cracked pipes by the extended finite element (XFEM) approach [19].

The extended finite element method (XFEM) has emerged as an alternative method with limited additional degrees of freedom, associated with the enrichment functions, to increase the accuracy of fracture analysis by FEM and to avoid mesh generation and adaptation difficulties [20–22]. These advantages make XFEM as an attractive method for a wide range of problems involving strong and weak discontinuities and crack tip singularities, such as cracking in composite structures [23–26].

Moreover, substantial improvement has been reported by applying XFEM to simulate through and interlaminar cracks in the shell structures [27]. Bayesteh and Mohammadi [19] utilized XFEM to simulate cracked isotropic shell and used COD and CTOA as a fracture criteria to show the accuracy and mesh independency of the method. XFEM was also used for linear buckling analysis for unilayer composite plates and cracked FGM cylindrical shells [28, 29]. Nasirmanesh and Mohammadi [30] also used XFEM for linear buckling and vibration analysis for unilayer composite plates and cracked FGM cylindrical shells. There is, however, a very limited literature on XFEM analysis of FRP repaired cracked pipes. Zarrinzadeh et al. [31] modeled the crack growth under fatigue tension loading on cracked repaired pipes with the composite wrap through the numerical XFEM modeling and experimental test.

Different crack criteria can be employed for the integrity assessment and crack propagation of pipelines. To model crack propagation, different measures including the energy release rate, the J-integral, the crack tip opening displacement (CTOD) and the crack tip opening angle (CTOA) were examined in different studies [32, 33]. The concept of leak before break (LBB) was also developed and applied for structural integrity assessment in oil and gas pipelines, pressure vessels, ships, nuclear piping, etc. [34].

In this study, a cracked API 5 L X65 pipe is simulated by the XFEM approach. CTOA is used as a fracture criterion for crack propagation assessment and COD is adopted as a parameter to assess the pipeline integrity and LBB analysis. Moreover, performances of different types of FRP repair systems and corresponding fracture criteria are investigated.

The structure of the paper is organized as follows; the basics of adopted shell element and the extended finite element method are presented in Section 2. Numerical simulations are then presented for crack propagation and LBB analysis and the effects of material properties and fiber orientations of the composite repair system on fracture parameters are investigated in Section 3.

2. Numerical method

The extended finite element method is a powerful numerical approach for analysis of weak or strong discontinuities without the need for discontinuities to match the finite element edges and no remeshing is required for propagation problems [19, 20]. In this method, first the conventional finite element mesh is generated (regardless of the existence of crack) and then a few degrees of freedom are added to the FE model in the nodes of elements which contain a crack edge (split nodes) or a crack tip (tip nodes), as depicted in Figure 1.

Eight-node shell elements are used in this study [19]. Geometry of an eight node shell element can be expressed as [35],

$$\mathbf{x}(r,s,t) = \sum_{i=1}^{8} N_i(r,s)\{\mathbf{x}_i + M_i(t)\boldsymbol{G}_i\} \tag{1}$$

where $N_i(r,s)$ are the conventional two dimensional FE shape functions and $M_i(t)$ represents the following one dimensional shape function:

$$M_i(t) = \frac{th_i}{2} \tag{2}$$

where h_i and G_i are the shell thickness and the unit outward vector at node i, respectively.

$$G_i = \frac{\mathbf{x}^{top} - \mathbf{x}^{bot}}{\|\mathbf{x}^{top} - \mathbf{x}^{bot}\|} \tag{3}$$

Now, assume there is a discontinuity or singularity in an arbitrary eight node shell element, as depicted in Figure 2. In the extended finite element method, the displacement for a point $\mathbf{x}$ inside the element is composed of two parts [20, 36]:

$$u^h(\mathbf{x}) = u^{FE} + u^{enr} \tag{4}$$

where u^{FE} is the classical finite element displacement field [35], and is expressed with

$$u^{FE}(\mathbf{x}) = \sum_{i=1}^{8} N_i(r,s)\left\{\hat{\mathbf{u}}_i - M\hat{\alpha}_i\mathbf{e}_{1i} + M\hat{\beta}_i\mathbf{e}_{2i}\right\} \tag{5}$$

or in the matrix form,

$$\begin{Bmatrix} u_1 \\ u_2 \\ u_3 \end{Bmatrix}^{FE} = \sum_{i=1}^{8} N_i(r,s)\left\{\begin{Bmatrix} u_{1i} \\ u_{2i} \\ u_{3i} \end{Bmatrix} - \frac{1}{2}th_i\hat{\alpha}_i\begin{Bmatrix} e^1_{1i} \\ e^2_{1i} \\ e^3_{1i} \end{Bmatrix} + \frac{1}{2}th_i\hat{\beta}_i\begin{Bmatrix} e^1_{2i} \\ e^2_{2i} \\ e^3_{2i} \end{Bmatrix}\right\} \tag{6}$$

The nodal displacements $\hat{\mathbf{u}}_i$ and rotations $\hat{\alpha}_i$, $\hat{\beta}_i$ with respect to $\mathbf{e}_{2i}$ and $\mathbf{e}_{1i}$ are shown in Figure 2. $\mathbf{e}_{1i}$ and $\mathbf{e}_{2i}$ orthogonal vectors are perpendicular to G_i.

The enriched part of the displacement field at any point $\mathbf{x}$, $\mathbf{u}^{ENR}$, can be expressed in terms of the crack-split and the crack tip components, $\mathbf{u}^{he}$ and $\mathbf{u}^{tip}$, respectively. $\mathbf{u}^{he}$ is defined as [19]

$$\mathbf{u}^{he}(\mathbf{x}) = \sum_{i=1}^{nh}\left\{N_i(r,s)\left[H(\phi(\mathbf{x})) - H(\phi(\mathbf{x}_i))\right]\left[\mathbf{a}_i - M\theta_i^{\alpha}\times\mathbf{e}_{1i} + M\gamma_i^{\beta}\times\mathbf{e}_{2i}\right]\right\} \tag{7}$$

and

$$\begin{Bmatrix} u_1 \\ u_2 \\ u_3 \end{Bmatrix}^{he} = \sum_{i=1}^{8}\left\{N_i(r,s)\left[H(\phi(\mathbf{x})) - H(\phi(\mathbf{x}_i))\right]\left[\begin{Bmatrix} a_{1i} \\ a_{2i} \\ a_{3i} \end{Bmatrix} - \frac{1}{2}th_i\theta_i^{\alpha}\begin{Bmatrix} e^1_{1i} \\ e^2_{1i} \\ e^3_{1i} \end{Bmatrix} + \frac{1}{2}th_i\gamma_i^{\beta}\begin{Bmatrix} e^1_{2i} \\ e^2_{2i} \\ e^3_{2i} \end{Bmatrix}\right]\right\} \tag{8}$$

and

$$H(\phi) = sign(\phi) = \begin{cases} 1 & \forall\phi > 0 \\ -1 & \forall\phi < 0 \end{cases} \tag{9}$$

nh is the number of nodes associated with the crack face, θ_i^{α} and γ_i^{β} are rotational degrees of freedom with respect to local vectors $\mathbf{e}_2$ and $\mathbf{e}_1$ at node i, respectively, $\mathbf{a}_i$ is the vector of additional degrees of freedom for modeling crack faces by the Heaviside function $H(\mathbf{x})$. The signed distance function $\xi(\mathbf{x})$ is defined as:

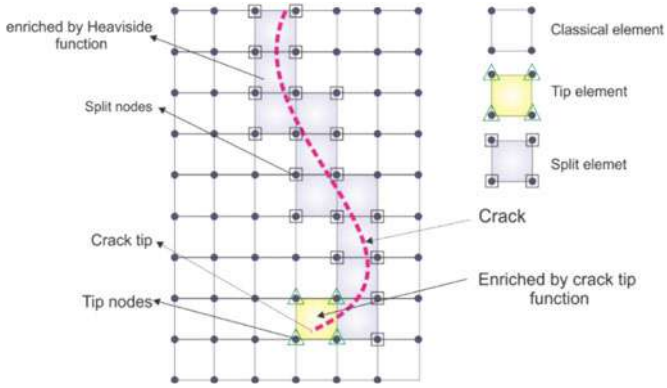

Figure 1. A typical XFEM modeling of a crack.

$$\xi(\mathbf{x}) = \min(\|\mathbf{x} - \mathbf{x}_\Gamma\|)sign(\mathbf{n}.(\mathbf{x} - \mathbf{x}_\Gamma)) \tag{10}$$

where $\mathbf{x}_\Gamma$ is the normal projection of $\mathbf{x}$ on Γ, and $\mathbf{n}$ is the unit normal vector, as depicted in Figure 3.

The crack tip displacement field can be expressed as,

$$u^{tip} = \sum_{1}^{8} N_i\left\{\sum_{l=1}^{nf}\left[(F_l - F_l(\mathbf{x}_i))\left({}^{F}\mathbf{b}_i^{lu}\right)\right] + \sum_{l=1}^{ng}\left[(G_l - G_l(\mathbf{x}_i))\left({}^{G}\mathbf{b}_i^{lu}\right)\right] + M\sum_{l=1}^{nr}\left[\left(R_l - R_l(\mathbf{x}_i)\left(-{}^{R}\mathbf{b}_i^{l\alpha}\mathbf{e}_2 + {}^{R}\mathbf{b}_i^{l\beta}\mathbf{e}_1\right)\right]\right\} \tag{11}$$

or (in the matrix form),

$$\begin{aligned}\{\mathbf{u}^{tip}\} = &\sum_{i=1}^{8} N_i\left\{\sum_{l=1}^{4}(F_l - F_l(\mathbf{x}_i))\begin{Bmatrix} b^l_{1i} \\ b^l_{2i} \\ 0 \end{Bmatrix}_i\right\} \\ &+ \sum_{i=1}^{8} N_i\left\{\sum_{l=1}^{1}(G_l - G_l(\mathbf{x}_i))\left(\begin{Bmatrix} 0 \\ 0 \\ b^l_{3i} \end{Bmatrix}\right)_i\right\} \\ &+ \sum_{i=1}^{8} N_i M\left[\sum_{l=1}^{4}(R_l - R_l(\mathbf{x}_i))\left(-b_i^{l\alpha}\begin{Bmatrix} e^1_{2i} \\ e^2_{2i} \\ e^3_{2i} \end{Bmatrix} + b_i^{l\beta}\begin{Bmatrix} e^1_{1i} \\ e^2_{1i} \\ e^3_{1i} \end{Bmatrix}\right)\right]\end{aligned} \tag{12}$$

where n_f, n_g and n_r are the number of in plane, out of plane and rotational tip enrichment functions, respectively, and $\mathbf{b}_k^l$ represents the vector of additional degrees of freedom to reproduce in plane, out of plane and rotational singularity at the crack tip.

The element stiffness matrix can then be computed as,

$$\mathbf{k}^{\mathbf{e}} = \int_{\Omega^e} \mathbf{B}^T\mathbf{D}\mathbf{B}d\Omega \tag{13}$$

where $\mathbf{B}$ is defined in terms of the derivatives of the shape functions and $\mathbf{D}$ is the material constitutive matrix.

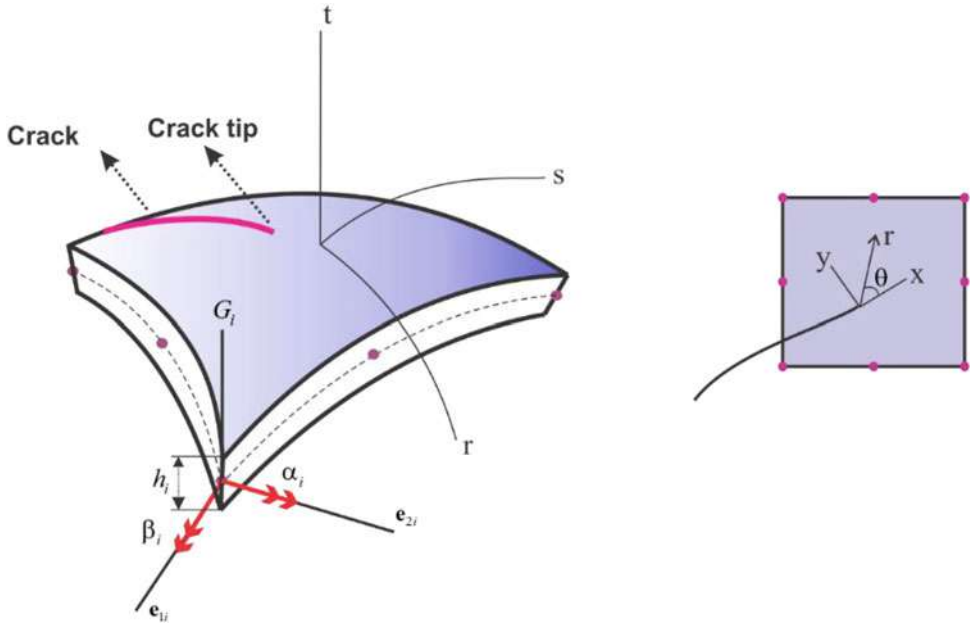

Figure 2. A typical 8-node shell element and definition of local coordinates on a node and at the crack tip.

F_l, G_l and R_l are the in plane, out of plane and rotational tip enrichment functions, respectively, derived from the analytical asymptotic displacement fields near the crack tip [19],

$$F(r,\theta) = \left\{ \sqrt{r}\sin\left(\frac{\theta}{2}\right), \sqrt{r}\cos\left(\frac{\theta}{2}\right), \sqrt{r}\sin\left(\frac{\theta}{2}\right)\sin(\theta), \sqrt{r}\cos\left(\frac{\theta}{2}\right)\sin(\theta) \right\} \tag{14}$$

$$G(r,\theta) = \left\{ \sqrt{r}\sin\left(\frac{\theta}{2}\right), r^{3/2}\sin\left(\frac{\theta}{2}\right), r^{3/2}\sin\left(\frac{3\theta}{2}\right), r^{3/2}\cos\left(\frac{3\theta}{2}\right), r^{3/2}\cos\left(\frac{3\theta}{2}\right) \right\} \tag{15}$$

$$R(r,\theta) = \left\{ \sqrt{r}\sin\left(\frac{\theta}{2}\right), \sqrt{r}\cos\left(\frac{\theta}{2}\right), \sqrt{r}\sin\left(\frac{\theta}{2}\right)\sin(\theta), \sqrt{r}\cos\left(\frac{\theta}{2}\right)\sin(\theta) \right\} \tag{16}$$

A simplified from of the out of plane enrichment which considers only the term proportional to $\sqrt{r}$ for u_3 is presented as [19]:

$$G(r,\theta) = \left\{ \sqrt{r}\sin\left(\frac{\theta}{2}\right) \right\} \tag{17}$$

Integration of the governing equations are performed by the 2×2 reduced Gauss quadrature rule for elements that are not cut by the crack. For cracked elements, the sub-triangulation technique is adopted [30] with 7 and 13 Gauss points in each triangle for the crack split and tip elements, respectively, as depicted in Figure 4.

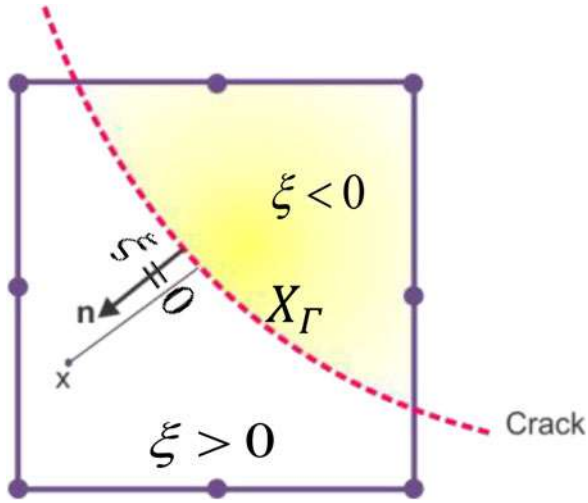

Figure 3. Definition of the signed distance function $sign(\phi)$.

3. Numerical simulations

In this section, linear fracture analyses are performed for a pipe in two conditions: the original cracked pipe and the composite-repaired cracked pipe. The effects of different parameters such as the internal pressure, crack length, fiber orientation and type of the composite repair system on fracture parameters, including the crack tip opening angle (CTOA), the crack opening displacement (COD) and the crack opening area (COA) are investigated. The problems include a pipe with a longitudinal crack and subjected to internal pressure. Boundary conditions and geometry of the pipe are presented schematically in Figure 5. The pipe and FRP are modeled with shell elements separately and a perfect bond is considered at the common interface degrees of freedom. The perfect bond assumption is consistent with practical FRP strengthening rules to avoid any delamination failure [31, 37].

3.1. CTOA and crack propagation for an API X65 pipe

Four different steel pipes with longitudinal crack and subjected to internal pressure P_{in} are simulated by the extended finite element method. The adopted finite element mesh, and the tip and Heaviside enriched elements are shown in Figure 6. Isotropic in-plane, out of plane and rotational tip enrichment functions are considered in all numerical simulations. Crack propagation is modeled based on the critical value of crack tip opening angle ($CTOA_c$). $CTOA_c$ has been adopted as a thickness independent fracture criterion to model quasi-static crack propagation problems [38]. Experimental values of $CTOA_c$ from different references for different steel pipelines and different specimens are shown in Table 1.

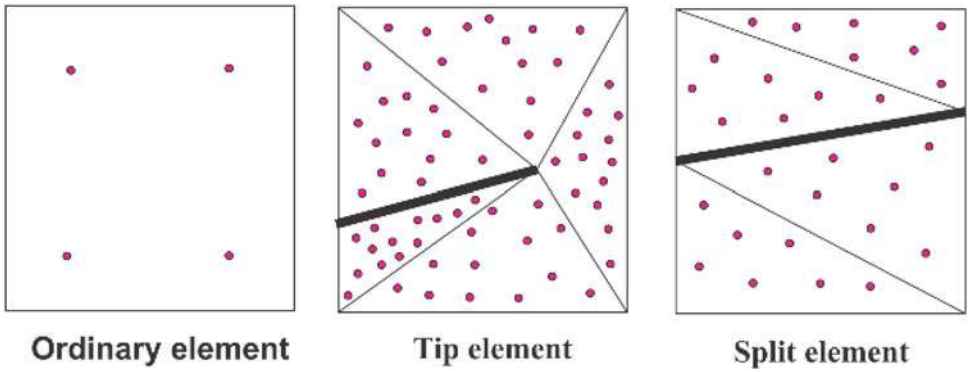

Figure 4. Various types of elements and Gauss points.

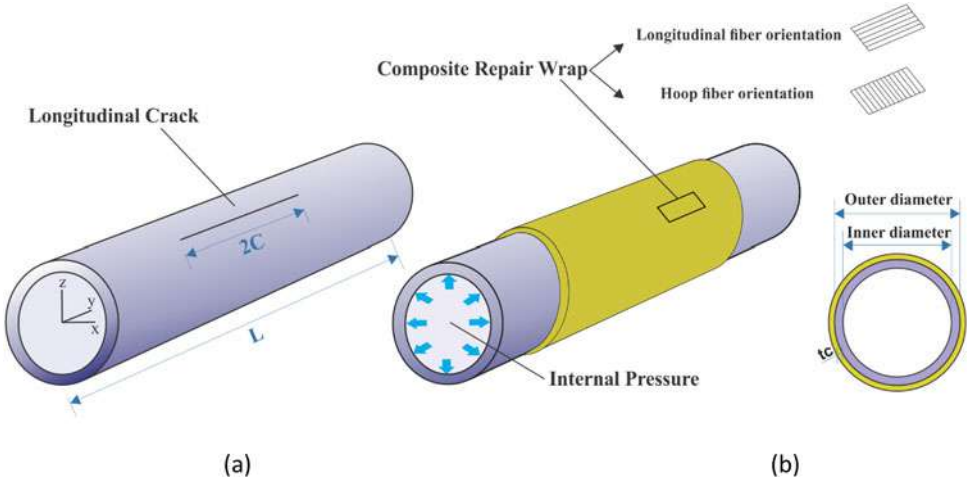

Figure 5. Geometry and boundary conditions for (a) bare cracked pipe, (b) repaired pipe, (c) section of repaired pipe.

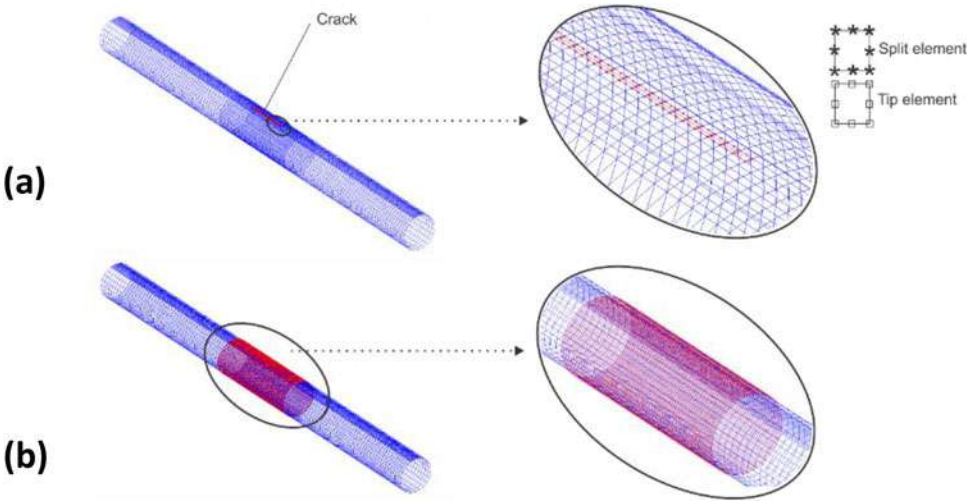

Figure 6. Finite element mesh (a) original cracked pipe (b) FRP repaired pipe.

For all cases, the thickness and outer diameter of pipes are t_c= 6.35 mm and D_O = 355 mm, respectively.

CTOA can be computed from the finite element solution by [19],

$$CTOA = 2\tan^{-1}\left(\frac{\delta_c}{2\delta_a}\right) \quad (18)$$

Figures 7a and b define δ_c, δ_a for FEM and XFEM solutions. Figure 8 depicts variations of internal pressure as a function of crack length for to different values of $CTOA_c$ (i.e. different pipe grades). Results show that the critical pressure (P_{cr}) before crack propagation increases with the increase of $CTOA_c$. Clearly, in each specimen, values of P_{cr} decrease as the crack length increases. So, internal pressure reduction is necessary in pipelines under operation before any repair procedure to avoid crack propagation.

Determination of critical operational pressure in cracked oil and gas pipelines especially in subsea pipelines is important to prevent crack extension due to internal pressure before repair. As observed, an API 5 L X65 pipe has the maximum value of critical operational pressure for any specific crack length. For example, for the crack length of 610 mm, values of P_{cr} for X65, X75, #1 and X100 pipes are 11, 8.25, 6.7 and 5 MPa, respectively. The internal pressure must be lower than this pressure to prevent crack extension.

Table 1. Values of $CTOA_c$ for different steel pipes.

Specimen	Reference	Steel pipe	Yield stress (MPa)	$CTOA_c$
MDCB	[39]	X65	448	20°
DWTT	[40]	X75	529	14.2°
Full-scale pipe	[38]	#1	543	11.61°
MDCB	[41]	X100	689	8.6°

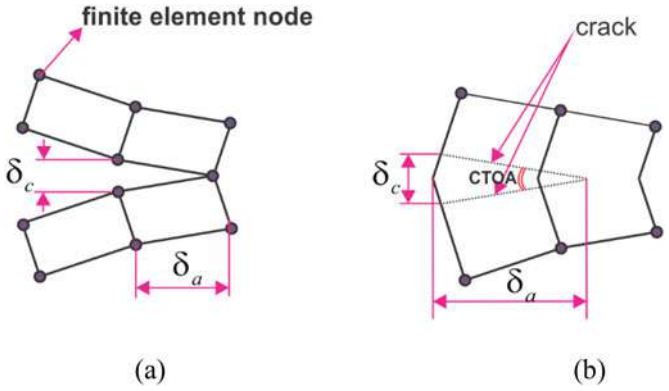

Figure 7. Definitions for calculating CTOA in (a) FEM, (b) XFEM.

3.2. Composite repaired pipe

In this section, the composite repair system is used as a solution to maintain the pipeline integrity. An API 5 L X65 pipe with an initial crack length of 2c = 600 mm is simulated. The length, outer diameter and thickness are 4570, 355, and 6.35 mm, respectively. The material properties are shown in Table 2.

The effects of four types of composite repair systems on CTOA are investigated. Two types of fiber reinforced composites: grade carbon/epoxy (C/E) and grade Gevetex E-glass/epoxy (G/E), each in two different fiber orientations are adopted, as defined in Tables 3 and 4

3.2.1. Effects of internal pressure

The values of CTOA of the original cracked pipeline and repaired pipeline with the four types of repair system at various internal pressures (15, 20, 25 MPa) are presented in Figure 9. Clearly, in a similar composite repair system and crack length, CTOA increases as the internal pressure increases. Moreover, the effect of pressure in both repaired and bare pipes remains similar.

3.2.2. Effects of composite repair system

Comparing the values of CTOA for different repaired pipelines with a constant repair thickness (Figure 9) shows that C/E laminates are more efficient than G/E laminates with the same fiber orientation. Moreover, the 0° fiber orientation angle provides the highest increase in resisting the crack propagation. Type 4 and Type 1 composite repair systems are the strongest and weakest reinforcement to decrease the CTOA, respectively. In the case of P_{in} =15 MPa, Type 4 and Type 1 repair systems decrease CTOA by 99% and 81% with respect to the original cracked pipe, respectively. The values of CTOA reduction are very similar in other internal pressures. The order of efficiency

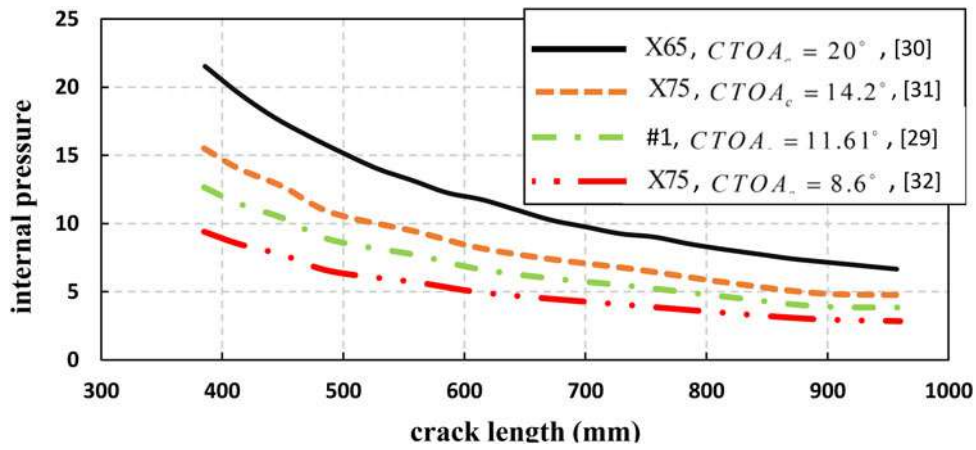

Figure 8. Pressure versus crack length for different $CTOA_c$.

for different composite repair types are Type 4, Type 3, Type 2, and Type 1, respectively.

3.2.3. Effects of laminate thickness

Figure 10 presents the values of CTOA in terms of FRP thickness at different values of pressure (15, 20, 25 MPa). It shows that the C/E (0°) repair can be efficient with the lowest thickness in comparison with other repair systems (due to its higher stiffness). Moreover, increase of the repair thickness t_c can significantly affect the repair performance by reducing CTOA and higher resistance to crack growth. A 67% decrease occurs in the value of CTOA for the case of P_{in} =15 MPa and Type1 repair system, as the t_c is increased from 1 to 5 mm. The reduction of CTOA decreases to 41%, as the repair thickness is increased from 5 to 10 mm. In addition, the results show a decreasing trend of the thickness effectivness as the repair thickness increases from 5 to 10 mm. Results show that increasing the thickness of Type1 composite repair system has the most effect on increasing trend of CTOA.

Table 2. Material properties of API 5L X65 [42].

Young's modulus, E (GPa)	207
Poisson's ratio	0.3

Table 3. Mechanical properties of FRP [43].

Fiber type	C/E	G/E
Matrix	3501-6 epoxy	LY556/HT907/DY063 epoxy
Specification	Prepreg	Filament winding
Manufacturer	Hercules	DLR
Fiber volume fraction, V_f	0.6	0.62
Longitudinal modulus $E_1(GPa)$	126	53.48
Transverse modulus, $E_2(GPa)$	11	17.7
In-plane shear modulus, G_{12} (GPa)	6.6	5.83
Major Poisson's ratio, υ_{12}	0.28	0.278
Through thickness Poisson's ratio, υ_{23}	0.4	0.4
Longitudinal tensile strength, X_T(MPa)	1950	1500
Longitudinal compressive strength, X_C(MPa)	1480	900
Longitudinal tensile failure strain, ε_{lT}(%)	1.38	1.080
Longitudinal compressive failure strain, ε_{lC}(%)	1.175	0.652

Table 4. Types of composite repair system.

Type	Fiber reinforced composite	Fiber orientation
1	G/E	90°(longitudinal orientation)
2	G/E	0°(hoop orientation)
3	C/E	90°(longitudinal orientation)
4	C/E	0°(hoop orientation)

3.3. COA and leak rate in cracked pipe

A cracked tube with the outer diameter of 19.05 mm and 1.07 mm thickness is now considered to determine the value of COD in the middle of the crack. The Yield stress and Young's modulus of the pipe are 241 MPa and 207 GPa, respectively. The crack length is set to 5, 5.5, and 6 mm [44].

Variations of normalized COD by half of the crack length versus the applied internal pressure at different crack lengths are presented in Figure 11. Comparing the results with reference [44] shows a good agreement, which further illustrates the accuracy of proposed modeling approach.

3.4. Analysis of leak rate for API X65 cracked pipeline

To study the potential for leakage in an oil/gas pipeline, an API X65 pipe with outer diameter of 822.6 mm and thickness of 25.4 mm is considered to contain an initial crack. The crack opening area (COA) and flow rate are important for leak study (before strength assessment) [45]. It is important to determine the crack opening area (COA) as a function of crack size and internal pressure to determine the capacity rate of leak of production. Other parameters such as the load level, possible influence of residual stresses, crack surface roughness and marine growth, which may also affect the flow rate [45], are not studied here.

In order to show the effects of pressure and crack length on the crack mouth deformation and leak rate, an XFEM analysis is performed for different pressures (14, 18, 22 and 26 MPa) and crack lengths (2c = 400, 500, and 600 mm). Figure 12 shows the crack opening displacement, perpendicular to the crack length, at half of the crack length. For the case of 2c = 600 mm, maximum displacement of the crack opening at the crack center (COD_m) decreases 46%, as the pressure is reduced from P_{in} =26 MPa to P_{in} =14 MPa.

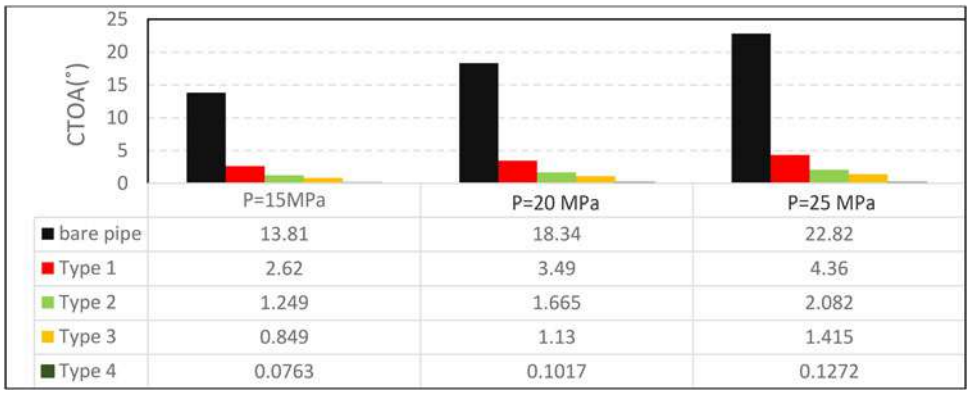

Figure 9. CTOA values in different pressures.

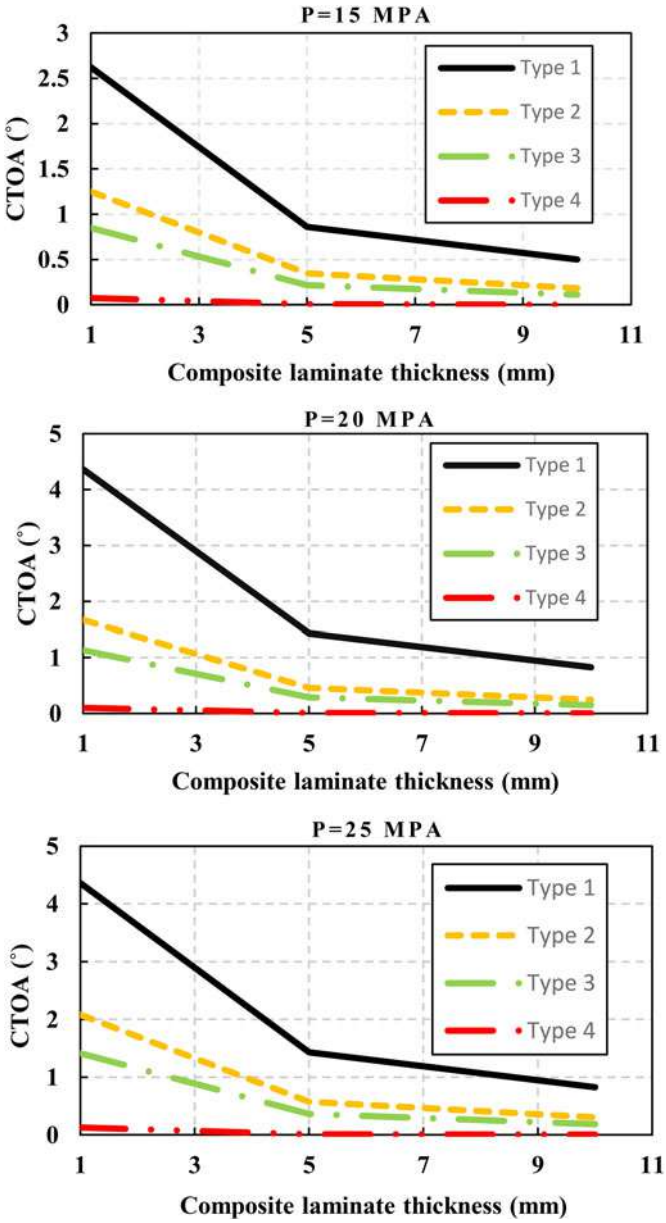

Figure 10. CTOA for different composite types and laminate orientations vs. the pressure for different FRP thicknesses.

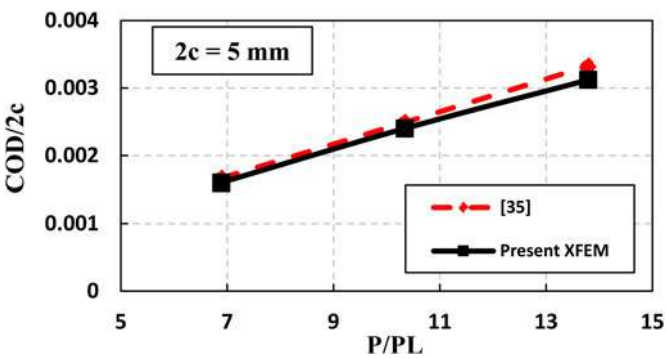

Figure 11. Variations of normalized COD for different crack lengths.

Also, for all cases P_{in}, COD_m increases 64% as the crack length is increased from 2c = 400 mm to 2c = 600 mm.

Figure 13 depicts the values of COA in terms of internal pressure at different values of crack lengths. Clearly, COA

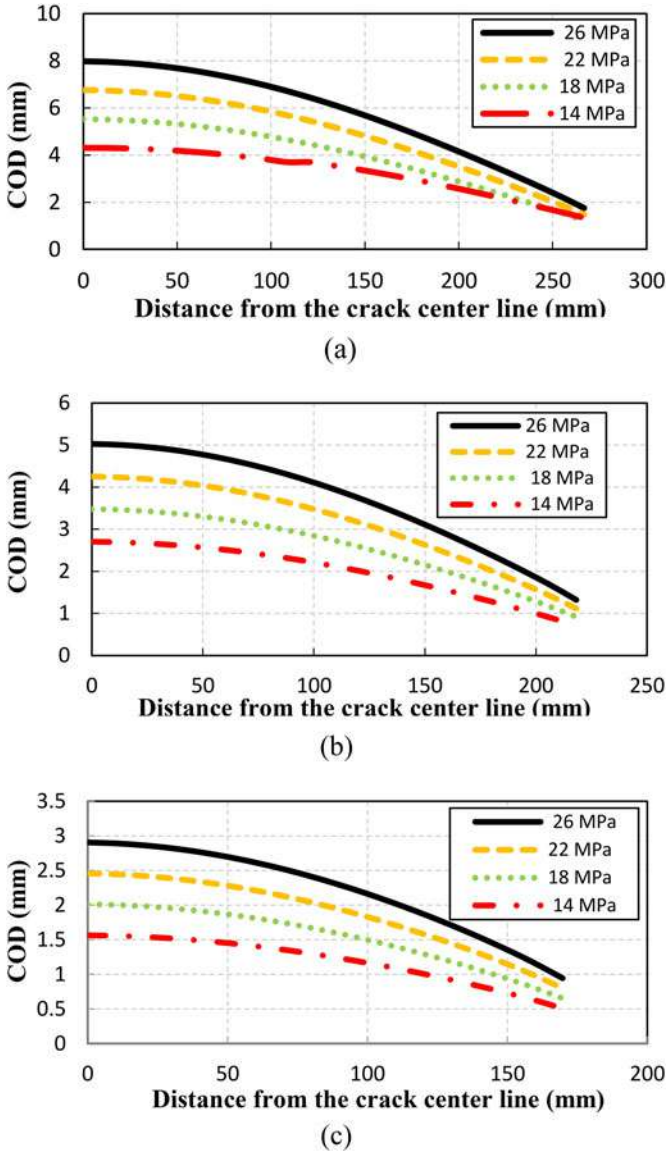

Figure 12. Crack opening displacement for different internal pressures, (a) 2c = 400 (b) 2c = 500 (c) 2c = 600 mm.

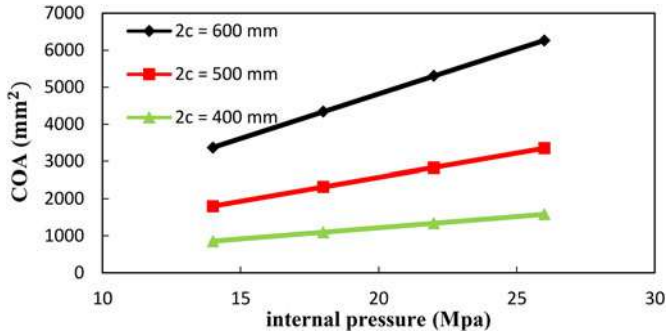

Figure 13. Crack opening area versus internal pressure for different crack lengths.

increases as the internal pressure increases at different crack lengths, i.e. COA increases 46% as the internal pressure increases from 14 MPa to 26 MPa in the case of 2c = 600 mm. Results show the increasing trend of COA with the crack length increases. A decrease of 50% occurs in the increasing slope of COA for the 100 mm shorter crack length.

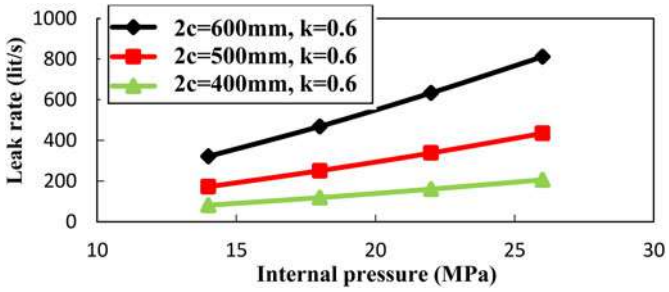

Figure 14. Flow rate versus internal pressure.

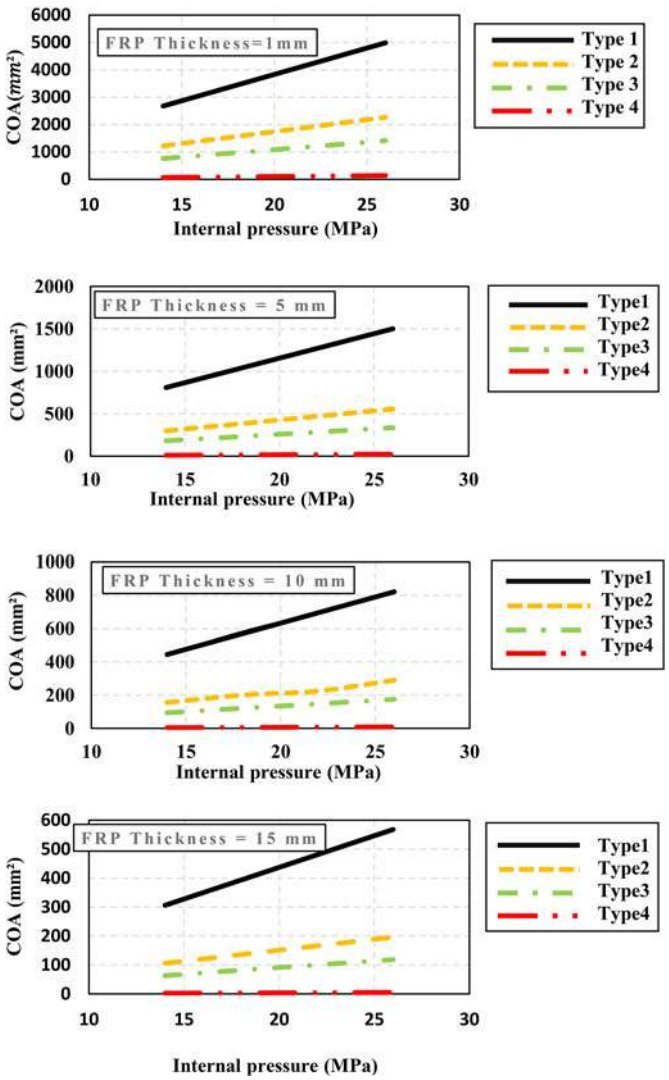

Figure 15. COA for different composite types vs. the pressure for different values of FRP thickness.

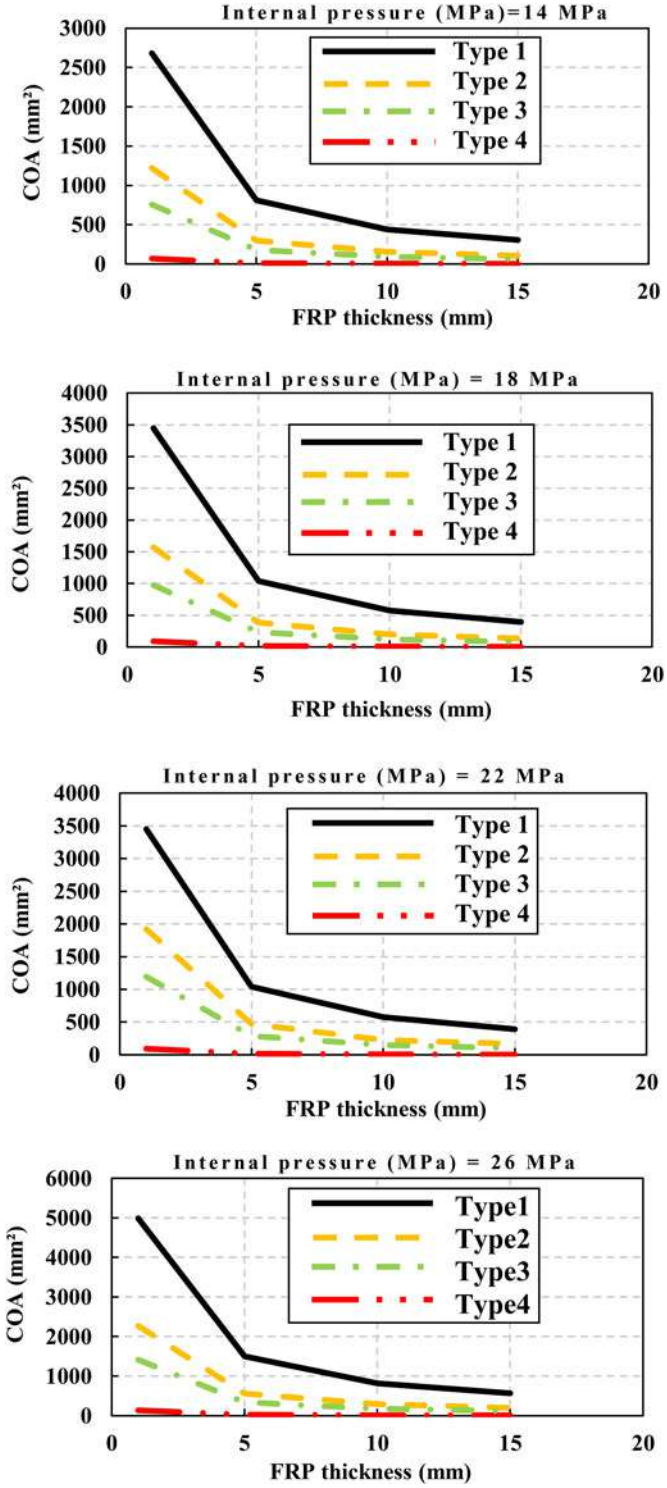

Figure 16. COA for different composite types vs. FRP thickness for different pressures.

It is well known that COA cannot solely determine the state of leakage in a through-thickness cracked pipe [45]. The flow rate also plays an important role and can be approximated by the well-known single phase flow (Bernoulli model) to determine the leak rate Q [45]

$$Q = k \times COA\sqrt{\frac{2\Delta P}{\rho}}$$

where k is an experimental flow coefficient, ΔP (Pa) is the pressure difference and ρ (kg/m^3) is the fluid density. The relationship between the flow rate and the internal pressure for different crack lengths are shown in Figure 14, which shows that the crack length can significantly change the increasing trend with the increase of crack length. As a result, the COA for the case of $2c = 600$ mm and $P_{in} = 26$ MPa is about 2 times greater than the case of $2c = 500$ mm. Moreover, the increasing trend of leak rate in terms of the internal pressure shows that the internal pressure reduction is necessary in pipelines under

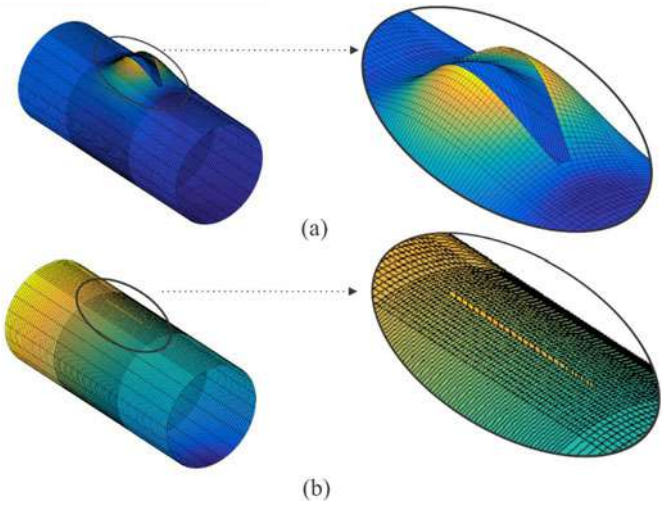

Figure 17. Deformed configurations of a) bare cracked pipe b) composite repaired pipe (magnified by 3).

operation before any repair procedure to avoid leak rate increase.

3.5. The effect of composite laminate on pipe integrity

The effects of four types of composite repair methods of Table 4 on the value of COA are now investigated. The length of the longitudinal crack is set to 600 mm.

Figure 15 illustrates variations of COA for the four types of repaired pipe as a function of the internal pressure for different FRP thicknesses. Expectedly, COA increases with the increase of internal pressure, while its increasing trend decreases for all repair systems, with Type 4 as the most effective repair system. Clearly, as the repair thickness increases, the increasing rate of COA decreases. As a result, for the case of Type1 repair system, 70%, 45% and 30% reductions occur in the COA rate, as the repair thickness is increased from 1 to 5 mm, 5 to 10 mm, and 10 to 15 mm, respectively.

Figure 16 depicts the variations of COA in terms of FRP thickness at different values of pressure (14, 18, 22, 26 MPa). Clearly, the values of crack opening area decreases with the increase of FRP thickness, while the reduction rate of COA reduces as the FRP thickness increases. All the results show that the most effective composite type is AS4 with the 0° hoop fiber orientation (Type 1).

In order to show the effect of repair system on the crack opening area, the deformed mesh configurations of bare cracked and repaired pipe are presented in Figure 17 (for the case of $P_{in} = 26$ MPa, $2c = 600$ mm and use of Type1 as a repair system with). Different forms of crack opening before and after repair can be clearly observed.

4. Conclusions

Fracture response and integrity of pipes with longitudinal cracks were studied by XFEM modeling. XFEM was selected because of its efficiency and accuracy in crack propagation problems and avoiding the need for mesh to conform to crack faces or weak discontinuities in crack propagation problems. CTOA, COD and COA as fracture criteria were used for both the pipe integrity assessment and the potential age of leak before break criterion. As a general result, an efficient composite repair system would be necessary to prevent crack propagation and maintain pipeline integrity. The effects of four different types of FRP repair systems, Carbon/epoxy and E-glass composites with both circumferential and longitudinal fiber orientations, on the fracture criteria and structural integrity were investigated. Accordingly, the following conclusion can be made:

- Among the four types of steel pipe specimens, API 5L X65 has the maximum value of critical operation pressure for any specific crack length.
- The maximum allowable pressure before crack propagation increases with the increase of critical CTOA.
- The decreasing trend of P_{cr} in terms of crack length indicates that an internal pressure reduction is necessary in pipelines under operation before any repair procedure to avoid crack extension.
- Using composite FRP layers as a repair system reduces considerably the values of CTOA and COA.
- Based on the material properties and fiber orientations, C/E laminates are more efficient than G/E laminates and the 0° fiber orientation angle provides the highest resistance to crack propagation and leakage due to decrease in CTOA and COD.
- Expectably, the values of CTOA and COD are reduced by the increase of FRP thickness and the rates of CTOA and COD reduction decrease with the increase of laminate thickness.
- The most effective repair system is Type 1: carbon/epoxy fiber reinforced composite with hoop fiber orientation. Hence, the cost of repair can be reduced by thinner laminates of this type.
- The values of CTOA and COD increase by the increase of internal pressure and crack length while the fracture parameters is reduced by the increase of FRP thickness.
- The Leak rate of pipe increases by the internal pressure and the crack length. So internal pressure must be reduced for pipe in operation before using any repair methods.
- The Leak rate, as an important pipeline integrity criterion, is directly proportional to COD and COA parameters. Hence, to prevent leakage in cracked pipeline, it is necessary to reduce these parameters by using an appropriate FRP repair system. According to the results, Type 1 FRP repair system is the most effective system with the least thickness to prevent leakage in cracked pipelines.

Acknowledgment

This research work has been supported technically by the High Performance Computing Lab, School of Civil Engineering, University College of Tehran, which is gratefully acknowledged.

Disclosure statement

No potential conflict of interest was reported by the authors.

References

[1] B. B. Bouiadjra, H. Fekirini, B. Serier, and M. Benguediab, SIF for inclined cracks repaired with double and single composite patch, Mech. Adv. Mater. Struct., vol. 14, no. 4, pp. 303–308, 2007.

[2] G. Ji, Z. Ouyang and G. Li, Effects of bondline thickness on Mode-II interfacial laws of bonded laminated composite plate, Int. J. Fracture, vol. 168, no. 2, pp. 197–207, 2011.

[3] Q. Q. Yu, T. Chen, X. L. Gu, and X. L. Zhao, Boundary element analysis of edge cracked steel plates strengthened by CFRP laminates, Thin Walled Struct., vol. 100, pp. 147–157, 2016.

[4] T. Mally, A. Johnston, M. Chann, R. Walker, and M. Keller, Performance of a carbon-fiber/epoxy composite for the underwater repair of pressure equipment, Compos. Struct., vol. 100, pp. 542–547, 2013.

[5] C. Alexander and O. O. Ochoa, Extending onshore pipeline repair to offshore steel risers with carbon fiber reinforced composites, Compos. Struct., vol. 92, no. 2, pp. 499–507, 2010.

[6] N. Saeed, H. Baji, and H. Ronagh, Reliability of corroded thin walled pipes repaired with composite overwrap, Thin-Walled Struct., vol. 85, pp. 201–206, 2014.

[7] A. Shouman and F. Taheri, Compressive strain limits of composite repaired pipelines under combined loading states, Compos. Struct., vol. 93, no. 6, pp. 1538–1548, 2011.

[8] H. Costa, J. Reis, L. Paim, M. Silva, R. Junior, and V. Perrut, Failure analysis of corroded pipelines reinforced with composite repair systems, Eng. Failure Anal., vol. 59, pp. 223–236, 2016.

[9] S. Shadlou and F. Taheri, On the effectiveness of composites for repair of pipelines under various combined loading conditions: A computational approach using the cohesive zone method, J. Pressure Vessel Technol. Trans. ASME, vol. 139, no. 2, pp. 1–7, 2017.

[10] C. Alexander, Assessing the use of composite materials in reinforcing offshore risers and pipelines. In: ASME 2011 30th International Conference on Ocean, Offshore, and Arctic Engineering Rotterdam. vol. 4: pipeline and riser technology, pp. 110, 2011.

[11] M. Lesani, M. R. Bahaari, and M. M. Shokrieh, FRP wrapping for the rehabilitation of circular hollow section (CHS) tubular steel connections, Thin Walled Struct., vol. 90, pp. 216–234, 2015.

[12] P. H. Chan, K. Y. Tshai, M. Johnson, and S. Li, The flexural properties of composite repaired pipeline : Numerical simulation and experimental validation, Compos. Struct., vol. 133, pp. 312–321, 2015.

[13] P. Chan, K. Y. Tshai, M. Johnson, H. L. Choo, and S. Li, Finite element modelling of composite repair in offshore pipe riser, Adv. Mater. Res., vol. 559, pp. 2239–2242, 2012.

[14] ASME PCC-2 Repair of Pressure Equipment and Piping, part4-Article 4.1,2008.

[15] H. Hosseini-Toudeshky and E. Fadaei, Effects of composite patch geometry on collapse load of pressurized steel pipes with internal longitudinal flaws, Appl. Mech. Mater. Vols., vol. 152–154, pp. 381–386, 2012.

[16] F. Benyahia, A. Albedah, B. Bachir Bouiadjra, and M. Belhouari, A comparison study of bonded composite repairs of through-Wall cracks in pipes subjected to traction, Bending moment and internal pressure, AMR, vol. 1105, pp. 41–45, 2015.

[17] A. Achour, A. Albedah, F. Benyahia, B. A. B. Bouiadjra, and D. Ouinas, Analysis of repaired cracks with bonded composite wrap in pipes under bending, J. Pressure Vessel Technol. Trans. ASME, vol. 138, no. 6, pp. 2–7, 2016.

[18] M. Meriem-Benziane, Finite element analysis of the integrity of an API X65 pipeline with a longitudinal crack repaired with single- and double-bonded composites, Compos. Part B, 2015.[Please provide volume number and page range for Ref. [18.]]

[19] H. Bayesteh and S. Mohammadi, XFEM fracture analysis of shells : The effect of crack tip enrichments, Comput. Mater. Sci., vol. 50, no. 10, pp. 2793–2813, 2011.

[20] S. Mohammadi, XFEM Fracture Analysis of Composites, John Wiley & Sons, New York, 2012.

[21] P. Baiz, S. Natatrajan, S. Bordas, K. Pierre, and T. Rabczuk, Linear buckling analysis of cracked plates by SFEM and XFEM, J. Mech. Mater. Struct., vol. 6, no. 1, pp. 9–10, 2011.

[22] H. Khazal, H. Bayesteh, S. Mohammadi, S. S. Ghorashi, and A. Ahmed, An extended element free galerkin method for fracture analysis of functionally graded materials, Mech. Adv. Mater. Struct., vol. 23, no. 5, pp. 513–528, 2016.

[23] A. Asadpoure and S. Mohammadi, Developing newenrichment functions for crack simulation in orthotropic media by the extended finite element method, Int. J. Numer. Methods Eng., vol. 69, no. 10, pp. 2150–2172, 2007.

[24] K. Khatri and A. Lal, Stochastic XFEM based fracture behavior and crack growth analysis of a plate with a hole emanating cracks under biaxial loading, Theor. Appl. Fracture Mech., vol. 96, pp. 1–22, 2018.

[25] A. Afshar, S. H. Ardakani, and S. Mohammadi, Stable discontinuous space – time analysis of dynamic interface crack growth in orthotropic bi-materials using oscillatory crack tip enrichment functions, Int. J. Mech. Sci., vol. 140, pp. 557–580, 2018.

[26] A. Afshar, S. Hatefi Ardakani, S. Hashemi, and S. Mohammadi, Numerical analysis of crack tip fields in interface fracture of SMA/elastic bi-materials, Int. J. Fracture, vol. 195, no. 1–2, pp. 39–52, 2015.

[27] D. H. Li, Delamination and transverse crack growth prediction for laminated composite plates and shells, Comput. Struct., vol. 177, pp. 39–55, 2016.

[28] A. Nasirmanesh and S. Mohammadi, XFEM buckling analysis of cracked composite plates, Compos. Struct, vol. 131, pp. 333–343, 2015.

[29] A. Nasirmanesh and S. Mohammadi, An extended finite element framework for vibration analysis of cracked FGM shells, Compos. Struct., vol. 180, pp. 298–315, 2017.

[30] A. Nasirmanesh and S. Mohammadi, Eigenvalue buckling analysis of cracked functionally graded cylindrical shells in the framework of the extended finite element method, Compos. Struct., vol. 159, pp. 548–566, 2017.

[31] H. Zarrinzadeh, M. Z. Kabir, and A. Deylami, Experimental and numerical fatigue crack growth of an aluminium pipe repaired by composite patch, Eng. Struct., vol. 133, pp. 24–32, 2017.

[32] J. C. Newman, M. A. James, and U. Zerbst, A review of the CTOA/CTOD fracture criterion, Eng. Fract. Mech., vol. 70, no. 3-4, pp. 371–385, 2003.

[33] X. Zhu, Review of fracture toughness test methods for ductile materials in low-constraint conditions, Int. J. Presure Vessel. Piping, vol. 138–139, pp. 173–183, 2016.

[34] G. Wilkowski, Leak-before-break: What does it really mean? J. Press. Vessel Technol., vol. 122, no. 3, pp 267–272, 2000.

[35] C. S. Krishnamoorthy, Finite Element Analysis: Theory and Programming, Tata McGraw-Hill Education, New York, 1995.

[36] S. Mohammadi, Extended Finite Element Method: for Fracture Analysis of Structures, Wiley/Blackwell, New York, 2008.

[37] M. Lesani, M. R. Bahaari, and M. M. Shokrieh, Numerical investigation of FRP-strengthened tubular T-joints under axial compressive loads, Compos. Struct., vol. 100, pp. 71–78, 2013.

[38] P. P. Darcis, C. N. McCown, H. Windhoff, J. D. McColskey, and T. A. Siewert, Crack tip opening angle optical measurement methods in five pipeline steels, Eng. Fracture Mech., vol. 75, no. 8, pp. 2453–2468, 2008.

[39] I. C. Guy. Pluvinage, Crack tip opening angle as a fracture resistance parameter to describe ductile crack extension and arrest in steel pipes, Phys. Mesomech., vol. 18, pp. 355–369, 2015.
[40] P. E. O'Donoghue, M. F. Kanninen, G. Demofoni, and S. Venzi, The development and validation of a dynamic fracture propagation model for gas transmission pipelines, Int. J. Pressure Vessel. Piping, vol. 70, pp. 11–25, 1997.
[41] R. L. Amaro, J. W. Sowards, E. S. Drexler, J. D. McColskey, and C. McCowan, CTOA testing of pipeline steels using MDCB specimens, J. Pipeline Eng.. pp. 199–214, 2013.
[42] M. Meriem-Benziane, S. A. Abdul-Wahab, H. Zahloul, B. Babaziane, M. Hadj-Meliani, and G. Pluvinage, Finite element analysis of the integrity of an API X65 pipeline with a longitudinal crack repaired with single- and double-bonded composites, Compos. Part B, vol. 77, pp. 431–439, 2015.
[43] P. H. Chan, K. Y. Tshai, M. Johnson, and S. Li, Finite element analysis of combined static loadings on offshore pipe riser repaired with fibre-reinforced composite laminates, J. Reinforced Plast. Compos., vol. 33, pp. 514–525, 2013.
[44] J. Jeong, S. Yu, Y. Chang, Y. Kim, S. Hwang, and H. Kim, Investigation on leak rate of steam generator tubes with multiple cracks, Trans. Korean Nucl. Soc. Autumn Meet. vol. 39, pp. 25–26, 2007.
[45] X. B. Ren, B. Nyhus, H. L. Lange, and M. Hauge, Leak-before-break analysis of a pipe containing circumferential defects, Eng. Failure Anal., vol. 58, pp. 369–379, 2015.